

# 1 **Enhanced risk of concurrent regional droughts with increased ENSO** 2 **variability and warming**

3

4 Jitendra Singh<sup>1\*</sup>, Moetasim Ashfaq<sup>2+</sup>, Christopher B. Skinner<sup>3</sup>, Weston B. Anderson<sup>4</sup>, Vimal  
5 Mishra<sup>5,6</sup>, Deepti Singh<sup>1</sup>

6

7 <sup>1</sup>School of the Environment, Washington State University, Vancouver, WA, USA.

8 <sup>2</sup>Computational Sciences and Engineering Division, Oak Ridge National Laboratory, Oak Ridge,  
9 TN, USA.

10 <sup>3</sup>Department of Environmental, Earth and Atmospheric Sciences, University of Massachusetts  
11 Lowell, Lowell, MA, USA.

12 <sup>4</sup>International Research Institute for Climate and Society, Columbia University, Palisades, NY,  
13 USA.

14 <sup>5</sup>Civil Engineering, Indian Institute of Technology (IIT) Gandhinagar, Gandhinagar, Gujarat,  
15 India

16 <sup>6</sup>Earth Sciences, Indian Institute of Technology (IIT) Gandhinagar, Gandhinagar, Gujarat, India

17

18 \*Corresponding author, Email: [jitendra.singh@wsu.edu](mailto:jitendra.singh@wsu.edu)

19

20

## 21 **Abstract:**

22 **Spatially compound extremes pose substantial threats to globally interconnected social-**  
23 **economic systems. We use an Earth system model large ensemble to examine the future**  
24 **risk of compound droughts during the boreal summer over ten global regions with highly**  
25 **seasonal climate. Relative to the late-20<sup>th</sup> century, the probability, mean extent and severity**  
26 **of compound droughts increase by ~60%, ~10% and ~20% respectively by the late-21<sup>st</sup>**  
27 **century, with a disproportionate increase in risk across North America and the Amazon.**  
28 **These changes result in a ~9-fold increase in exposure over agricultural areas and ~5 to 20-**  
29 **fold increase in population exposure depending on the shared socioeconomic pathway.**  
30 **ENSO is the predominant large-scale driver of compound droughts with 68% of historical**  
31 **events occurring during El Niño or La Niña conditions. ENSO teleconnections remain**

---

+ This manuscript has been co-authored by employees of Oak Ridge National Laboratory, managed by UT Battelle, LLC, under contract DE-AC05-00OR22725 with the U.S. Department of Energy. The publisher, by accepting the article for publication, acknowledges that the United States Government retains a non-exclusive, paid-up, irrevocable, world-wide license to publish or reproduce the published form of this manuscript, or allow others to do so, for United States Government purposes. The Department of Energy will provide public access to these results of federally sponsored research in accordance with the DOE Public Access Plan (<http://energy.gov/downloads/doe-public-access-plan>)

32 **stationary in the future though an ~22% increase in ENSO extremes combined with**  
33 **projected warming, drive the elevated risk of compound droughts.**  
34  
35

36 Spatially and/or temporally compounding Earth system extremes can lead to cascading impacts  
37 on global socio-economic systems<sup>1-6</sup>. Several recent studies have examined temporally  
38 compounding events resulting from different combinations of climatic hazards occurring in the  
39 same location at the same time, such as hot and dry conditions<sup>7,8</sup> or heavy precipitation and  
40 extreme winds<sup>9</sup>. The simultaneous occurrence of extremes across multiple regions, referred to as  
41 spatially compound extremes, have received relatively limited attention. Spatially compound  
42 extremes have the potential to accumulate hazard impacts in distant locations and pose  
43 amplifying pressures on a network of interconnected socioeconomic systems<sup>1,10-15</sup>. For example,  
44 severe droughts that concurrently occurred across Asia, Brazil, and Africa during 1876 to 1878  
45 led to synchronous crop failures, followed by famines that killed more than 50 million people in  
46 those regions<sup>16</sup>. The complex and interconnected nature of the current global food network  
47 makes agricultural shocks, even over a few individual regions, capable of having ripple effects  
48 on global food prices and food security, particularly in socioeconomically vulnerable regions<sup>11,17</sup>.  
49 Compound extremes can also influence global economies through their impacts on international  
50 agribusiness and reinsurance industries<sup>7,18,19</sup>. Therefore, understanding the drivers of  
51 simultaneous extremes across regions and the exposure of human systems to such extremes can  
52 inform assessments of the climate risks to interconnected systems and planning for their societal  
53 impacts.

54 Recent studies have examined the risk of crop failures from compound extremes and highlighted  
55 various physical drivers and mechanisms. The risk of multiple-breadbasket failures is elevated  
56 during the simultaneous physical hazards imposed by the large-scale natural climate variability  
57 modes such as El Niño-Southern Oscillation (ENSO), Indian Ocean Dipole, and Atlantic  
58 Niño<sup>12,13,20</sup>. ENSO is one of the predominant drivers of hydroclimate variability across tropical  
59 regions, as El Niño events are associated with several major synchronous historical droughts  
60 across Asia, Africa and South America<sup>16,21</sup>. For instance, the strong El Niño event in 1983  
61 caused extreme heatwaves and droughts across multiple maize-producing regions that resulted in  
62 the most extensive simultaneous crop failures in recent records<sup>13,17</sup>. Overall, ~80% of historical  
63 compound droughts over tropical/subtropical belt are associated with El Niño conditions during  
64 the boreal summer<sup>20</sup>. Projected anthropogenic warming is expected to double the risk of  
65 concurrent hot and dry extremes over certain croplands and pastures<sup>7</sup> and enhance the risk of  
66 globally synchronized shocks on temperature-sensitive crops such as Maize<sup>15</sup>, highlighting the  
67 importance of understanding the drivers of compounding stressors.

68 This study aims to understand future changes in the characteristics and drivers of spatially  
69 compounding droughts (hereafter compound droughts) that could result in simultaneous shocks  
70 across multiple regions, highlighting the increasing risks to a suite of climate-sensitive sectors  
71 and systems. Our analysis focuses on ten tropical and subtropical regions, defined in the  
72 Intergovernmental Panel on Climate Change (IPCC) Special Report on Managing the Risks of  
73 Extreme Events and Disasters to Advance Climate Change Adaptation (SREX), that exhibit high  
74 variability in summer precipitation and receive a large fraction of their annual precipitation  
75 during their summer season. Several of these regions exhibit similar socioeconomic and climate  
76 characteristics, including areas where rainy seasons and agricultural production are strongly

77 influenced by the global monsoon systems. These regions also include important breadbaskets  
78 and vulnerable populations that depend on rainfed agriculture for their livelihood<sup>22,23</sup>. Given the  
79 importance of ENSO for hydroclimate variability over many of these regions<sup>13,16,24-27</sup>, we  
80 investigate the influence of El Niño and La Niña events on compound drought characteristics in  
81 the historical and future climates. We also quantify changes in the population and agricultural  
82 land exposure to compound droughts to understand societal implications of projected changes.

83

84 **Historical and future characteristics of compound droughts.** We find significant increases in  
85 the frequency, spatial extent, and average intensity of compound droughts in the late-21<sup>st</sup> century  
86 (2071–2100) relative to the late 20<sup>th</sup> century (1971–2000) in the Community Earth System Model  
87 Large Ensemble simulations for the high-emissions Representative Concentration Pathway 8.5  
88 (Figure 1). The number of regions simultaneously under drought is significantly ( $p$ -value $<0.05$ )  
89 higher in the future relative to the historical climate (Figure 1b), contributing to a ~60% increase  
90 in the probability of compound droughts (historical probability = 0.32 and future probability =  
91 0.51). The fraction of drought-affected area during compound droughts is also significantly  
92 higher in the future climate, with the probability of widespread compound droughts increasing by  
93 ~30% relative to the historical climate (Figure 1c). Likewise, the mean severity of compound  
94 droughts also increases (Figure 1d) along with the probability of severe compound droughts,  
95 which increases ~6-fold from 0.12 in the historical climate to 0.75 in the future climate. As a  
96 result, nearly 3 out of 4 compound droughts in the future are classified as severe (Figure 1d).

97 We quantify the impacts of more frequent, extensive and severe compound droughts on  
98 agricultural land (the combination of cropland and pastureland) and population by calculating  
99 changes in their exposures to compound droughts (Figure 2). These exposures exhibit distinct  
100 differences between the two climates and are sensitive to drought severity. While agriculture  
101 areas exposed to moderate compound droughts in the historical climate is twice as high as in the  
102 future climate (Figure 2a), their exposure to severe compound droughts increases ~10-fold in the  
103 future climate. An average of ~0.7 million km<sup>2</sup> of agricultural land is likely to be exposed to  
104 severe compound droughts every year in the future climate compared to ~0.07 million km<sup>2</sup> in the  
105 historical climate (Figure 2a). Since the agricultural area does not change in the two analyses  
106 periods, the differences in exposure is largely driven by changes in the frequencies and extent of  
107 moderate and severe compound drought in the two time periods.

108 Increases in the severity of compound droughts in future climate is associated with changes in  
109 the characteristics of the water cycle. Specifically, several regions either exhibit a decrease in  
110 precipitation (CNA, CAM, and northern AMZ), or an increase in ET (northern CAM and ENA),  
111 both of which enhance surface drying (Figure S1c,d) and elevate the risk of compound droughts  
112 (Figure S2a). As a result, there is an increase in the likelihood of severe compound droughts  
113 exposure to agricultural lands within these regions (Figure 3a,b; Figure S2a,b). Alternatively, the  
114 decrease in agricultural exposure to moderate compound droughts over the EAS, SAS and EAF  
115 regions is due to an increase in summer precipitation in the future climate (Figure S1; Figure 3b).  
116 As a result, these regions are less likely to experience compound droughts in the future climate  
117 (Figure 3a). Although a reduction in agricultural exposure to compound droughts is projected  
118 over EAF, there is a considerable uncertainty in the response of EAF precipitation to warming<sup>28</sup>.

119 Differences in the distribution and growth of population in the five Shared Socioeconomic  
120 Pathways (SSPs) lead to substantially varying population exposures to compound droughts

121 (Figure 2b). Future population exposure to severe (moderate) compound droughts increases  
122 (declines) under all SSPs (Figure 2b). In the historical climate, an average of ~10 million people  
123 are at risk of experiencing severe compound droughts every year, which increases to an average  
124 of ~120 million people under SSP1 and SSP5, ~160 million under SSP2 and SSP4, and more  
125 than 210 million people under SSP3 every year by the late 21<sup>st</sup> century (Figure 2b). The  
126 exceptionally large increase in population exposure to severe compound droughts under SSP3 is  
127 primarily driven by a large increase in the frequency of severe compound droughts and in the  
128 population across all regions except SEA and EAS (Figure 3c; Figure S2c-f). Despite declines in  
129 compound droughts risk, the projected increase in population over EAF, WAF, and SAS  
130 contributes to increasing future population exposure<sup>29</sup> (Figure 3a).

131 **Physical drivers of compound droughts.** ENSO is the dominant mode of natural climate  
132 variability influencing compound droughts in the boreal summer season (Figure 4)<sup>16,20</sup>.  
133 Historically, ~68% of compound droughts are associated with significant ENSO events, of which  
134 El Niño conditions alone account for ~46% of compound droughts occurrences (Figure 4b). With  
135 the projected warming, ENSO events become more frequent, including a 30% increase in El  
136 Niño and 15% increase in La Niña conditions (Figure 4a). The more frequent occurrences of  
137 ENSO in the future warmer climate are consistent with previous studies<sup>30,31</sup>. In the future  
138 climate, ~75% of compound droughts are driven by ENSO variability, and the fraction of  
139 compound droughts associated with El Niño conditions increases to ~50% (Figure 4b). In total,  
140 compound droughts events associated with El Niño and La Niña conditions increase by ~70%,  
141 from 263 events in the historical climate to 448 in the future climate, in response to a ~22%  
142 future increase (from 712 to 869 events) in the frequency of ENSO events (Figure 4a, b). The  
143 frequency of compound droughts associated with non-ENSO drivers also exhibit a moderate  
144 increase of ~25% (Figure 4b). The proportional occurrence of compound droughts during El  
145 Niño and La Niña conditions is similar in both time periods (i.e., association with El Niño is ~2  
146 (1.96) times more than La Niña in the historical (future) climate) (Figures 4b). Collectively,  
147 these characteristics of future changes not only manifest as a stronger role of ENSO in driving  
148 summer season compound droughts, but also suggest that ENSO teleconnections over the study  
149 regions remain largely stationary.

150 The more prominent role of El Niño in driving spatially compound droughts is due to its negative  
151 correlation with precipitation variability over most of the studied regions. El Niño conditions  
152 lead to intense and widespread drying over CAM, AMZ, WAF, EAF, EAS, southern SAS, and  
153 SEA in the historical climate (Figure S3a). In contrast, La Niña conditions lead to drying over  
154 relatively fewer studied regions, including CNA, ENA, southern WAF, and northern SEA  
155 (Figure S3c). El Niño-driven compound droughts also exhibit relatively larger mean drought  
156 extent compared to La Niña-driven compound droughts in both climates, and compared to non-  
157 ENSO driven compound droughts in the historical climate (Figure 5a-c). While La Niña-driven  
158 compound droughts events exhibit higher intensity in the historical climate, more intense  
159 compound droughts are predominantly due to El Niño conditions in the late 21<sup>st</sup> century (Figure  
160 5c). In fact, El Niño-driven compound droughts not only have the highest mean severity in the  
161 future climate, but their extreme severity is also the highest among all the drivers (Figure 5c).  
162 These changes are consistent with relatively strong future climate drying during El Niño  
163 conditions (Figure S3). The composites of Standardized Precipitation Evapotranspiration Index  
164 (SPEI) during El Niño show an expansion of the drought area over AMZ and CAM, and an  
165 intensification of dry conditions over EAF and SEA in the future climate. Some intensification of

166 drying is also present during La Niña (non-ENSO) conditions over ENA, WAF and AMZ (CAM  
167 and AMZ) in the future climate (Figure S3c-f).

168

169 **ENSO Teleconnections.** We investigate changes in the influence of ENSO over the study  
170 regions by examining its teleconnections with SPEI (Figure 6) and precipitation anomalies across  
171 the study regions (Figure S4). The magnitude and pattern of correlations between the summer  
172 ENSO index and the SPEI/precipitation is very similar in both time periods, which highlights the  
173 fact that the ENSO teleconnections over most regions remain largely stable with the exception of  
174 ENA, WAF and EAF where correlations are stronger in the future climate (Figure 6a-b,d, S4).  
175 The area with a significant correlation between SPEI and ENSO over ENA increases from ~40%  
176 in the historical climate to ~70% in the climate (Figure 6c). Moreover, the average correlation  
177 over WAF (EAF) increases to ~0.35 (~0.4) in future climate relative to ~0.25 (~0.35) in the  
178 historical climate (Figure 6d). Corresponding to the relative strengthening of ENSO  
179 teleconnections, the SPEI composite shows stronger dry conditions over western EAF during El  
180 Niño conditions and over southern WAF and eastern ENA during La Niña conditions in the  
181 future climate (Figure S5). Similarly, wet conditions also exhibit strengthening over southern  
182 WAF and eastern ENA during El Niño, and over eastern EAF during La Niña conditions (Figure  
183 S4). Broadly, the nature of ENSO teleconnections remain stationary in the future climate, which  
184 highlights the importance of understanding the current ENSO-compound droughts relationship  
185 and their related physical processes<sup>20</sup>.

186

187 **Discussion.** Droughts are associated with a range of environmental, economic, and social  
188 impacts. Given the increasing global connectivity of socio-economic systems, understanding the  
189 historical characteristics of compound droughts and anticipating their changes in a future warmer  
190 climate is important for a broad suite of interconnected, climate-sensitive sectors<sup>7</sup>. The  
191 agricultural sector, in particular, is highly sensitive to simultaneous shocks across multiple  
192 regions because of the complex networks of food supply, demand and global trade<sup>6</sup>. The  
193 projected increase in agricultural exposure to compound droughts highlights the higher  
194 likelihood of simultaneous production shocks across multiple breadbaskets in the future period  
195 that could affect global food availability and security. Our results indicate that the North and  
196 South American regions, considered in this study, are more likely to experience compound  
197 droughts in a future warmer climate as compared to the regions in Asia and Africa, where much  
198 of the areas affected by monsoons are projected to become wetter<sup>32</sup>. The contribution of food  
199 produced within the Americas to the global food system could, therefore, be more susceptible to  
200 such climatic hazards. For instance, the United States is a major exporter of staple grains and  
201 currently exports maize (soyabean) to >160 (>90) countries across the globe<sup>11,33</sup>. Therefore, a  
202 modest increase in the risk of compound droughts in the future climate can lead to regional  
203 supply shortfalls that could cascade into the global market, affecting global prices and  
204 amplifying food insecurity. Additionally, our results have broader implications for the global  
205 virtual water trade network involved in the water-intensive agricultural, forestry, industrial, and  
206 mining products<sup>34,35</sup>. In last three decades, international trade of virtual water has tripled<sup>35</sup> and is  
207 expected to increase further in response to increases in population and demand by end of 21st  
208 century<sup>36</sup>. Therefore, the projected increases in the frequency and severity of compound droughts  
209 could disrupt the supply-demand network of such water intensive goods and thereby, can affect  
210 their availability and prices in global market.

211 In addition to impacts on such connected systems, the interplay of projected growth in  
212 population and changes in compound drought characteristics will also exacerbate direct  
213 population exposure to drought impacts. The largest increase in population exposure to severe  
214 compound droughts is projected under SSP3, which represents a fragmented future world of  
215 resurgent nationalism, low-income growth, focus on domestic or regional issues, and high  
216 population growth in developing countries<sup>29</sup>. Persistent inequality and low economic growth  
217 under SSP3 indicate societies that are likely less resilient to severe compound droughts and  
218 consequently might experience higher socio-economic impacts. In contrast, the increase in  
219 population exposure to compound drought is lowest under SSP1. SSP1 represents a trajectory  
220 of sustainable development, lower inequality, high economic growth, higher investment in  
221 human capital and a focus on global commons<sup>29</sup>, which might be better prepared to manage the  
222 impacts of compound droughts. Irrespective of the scenario, a warming climate will amplify  
223 stresses on international agencies responsible for disaster relief by requiring the provision of  
224 humanitarian aid to a greater number of people simultaneously exposed to drought-related  
225 disasters.

226 Efforts to better understand and constrain the hydroclimatic impacts of ENSO variability,  
227 however, can support predictability and management of compound drought impacts in a warmer  
228 climate. Our findings suggest that the regional teleconnections during El Nino or La Nina  
229 conditions do not change substantially, with increases mainly in the intensity of compound  
230 droughts in the future climate relative to historical climate. These results imply that when ENSO  
231 events occur, they will likely affect the same geographical regions albeit with greater severity.  
232 The occurrence of nearly 75% of compound droughts with ENSO events in the future climate  
233 highlights the potential for predictability of compound droughts and their impact at lead times of  
234 up to 9-months<sup>37</sup>. Timely predictions of compound droughts and their impacts on agricultural  
235 areas and communities can facilitate international agribusiness industries to minimize the  
236 economic losses and insurance and re-insurance industries to design effective insurance schemes  
237 to reduce losses from simultaneous disasters.

238

## 239 **References**

- 240 1. Zscheischler, J., Martius, O., Westra, S., Bevacqua, E. & Raymond, C. A typology of  
241 compound weather and climate events. *EGU Gen. Assem. 2020* EGU2020-8572 (2020)  
242 doi:<https://doi.org/10.5194/egusphere-egu2020-8572>.
- 243 2. Raymond, C. *et al.* extreme events. *Nat. Clim. Chang.* (2017) doi:10.1038/s41558-020-  
244 0790-4.
- 245 3. AghaKouchak, A. *et al.* Climate Extremes and Compound Hazards in a Warming World.  
246 *Annu. Rev. Earth Planet. Sci.* **48**, 519–548 (2020).
- 247 4. Zscheischler, J. *et al.* Future climate risk from compound events. *Nat. Clim. Chang.* **8**,  
248 469–477 (2018).
- 249 5. Leonard, M. *et al.* A compound event framework for understanding extreme impacts.  
250 *Wiley Interdiscip. Rev. Clim. Chang.* **5**, 113–128 (2014).
- 251 6. Raymond, C. *et al.* Understanding and managing connected extreme events. *Nat. Clim.*  
252 *Chang.* **10**, 611–621 (2020).

- 253 7. Sarhadi, A., Ausín, M. C., Wiper, M. P., Touma, D. & Diffenbaugh, N. S.  
254 Multidimensional risk in a nonstationary climate: Joint probability of increasingly severe  
255 warm and dry conditions. *Sci. Adv.* **4**, (2018).
- 256 8. Mishra, V., Thirumalai, K., Singh, D. & Aadhar, S. Future exacerbation of hot and dry  
257 summer monsoon extremes in India. *npj Clim. Atmos. Sci.* **3**, 1–9 (2020).
- 258 9. Raveh-Rubin, S. & Wernli, H. Large-scale wind and precipitation extremes in the  
259 Mediterranean: A climatological analysis for 1979-2012. *Q. J. R. Meteorol. Soc.* **141**,  
260 2404–2417 (2015).
- 261 10. Kornhuber, K. *et al.* Amplified Rossby waves enhance risk of concurrent heatwaves in  
262 major breadbasket regions. *Nat. Clim. Chang.* **10**, 48–53 (2020).
- 263 11. Heslin, A. *et al.* Simulating the Cascading Effects of an Extreme Agricultural Production  
264 Shock: Global Implications of a Contemporary US Dust Bowl Event. *Front. Sustain. Food*  
265 *Syst.* **4**, 1–12 (2020).
- 266 12. Anderson, W., Seager, R., Baethgen, W. & Cane, M. Trans-Pacific ENSO teleconnections  
267 pose a correlated risk to agriculture. *Agric. For. Meteorol.* **262**, 298–309 (2018).
- 268 13. Anderson, W. B., Seager, R., Baethgen, W., Cane, M. & You, L. Synchronous crop  
269 failures and climate-forced production variability. *Sci. Adv.* **5**, 1–10 (2019).
- 270 14. Gaupp, F., Hall, J., Hochrainer-stigler, S. & Dadson, S. Changing risks of simultaneous  
271 global breadbasket failure. *Nat. Clim. Chang.* (2019) doi:10.1038/s41558-019-0600-z.
- 272 15. Tigchelaar, M., Battisti, D. S., Naylor, R. L. & Ray, D. K. Future warming increases  
273 probability of globally synchronized maize production shocks. *Proc. Natl. Acad. Sci. U. S.*  
274 *A.* **115**, 6644–6649 (2018).
- 275 16. Singh, D. *et al.* Climate and the Global Famine of 1876-78. *J. Clim.* **31**, 9445–9467  
276 (2018).
- 277 17. Mehrabi, Z. & Ramankutty, N. Synchronized failure of global crop production. *Nat. Ecol.*  
278 *Evol.* **3**, 780–786 (2019).
- 279 18. Mills, E. Insurance in a climate of change. *Science (80-. )*. **309**, 1040–1044 (2005).
- 280 19. Levermann, A. Climate economics: Make supply chains climate-smart. *Nature* **506**, 27–29  
281 (2014).
- 282 20. Singh, J., Skinner, C. B. & Anderson, W. B. Amplified risk of spatially compounding  
283 droughts during co-occurrences of modes of natural ocean variability. *npj Clim. Atmos.*  
284 *Sci.* 1–14 doi:10.1038/s41612-021-00161-2.
- 285 21. Mishra, V. *et al.* Drought and Famine in India, 1870–2016. *Geophys. Res. Lett.* **46**, 2075–  
286 2083 (2019).
- 287 22. Kitoh, A. *et al.* Monsoons in a changing world: A regional perspective in a global context.  
288 *J. Geophys. Res. Atmos.* **118**, 3053–3065 (2013).
- 289 23. Byers, E. *et al.* Global exposure and vulnerability to multi-sector development and climate  
290 change hotspots. *Environ. Res. Lett.* **13**, (2018).
- 291 24. Han, T., Wang, H. & Sun, J. Strengthened relationship between eastern ENSO and

- 292 summer precipitation over Northeastern China. *J. Clim.* **30**, 4497–4512 (2017).
- 293 25. Kumar, K. K., Rajagopalan, B. & Cane, M. A. On the weakening relationship between the  
294 indian monsoon and ENSO. *Science (80-. )*. **284**, 2156–2159 (1999).
- 295 26. Silvestri, G. E. El Niño signal variability in the precipitation over southeastern South  
296 America during austral summer. *Geophys. Res. Lett.* **31**, 1–5 (2004).
- 297 27. Wang, B., Liu, J., Kim, H. J., Webster, P. J. & Yim, S. Y. Recent change of the global  
298 monsoon precipitation (1979-2008). *Clim. Dyn.* **39**, 1123–1135 (2012).
- 299 28. Rowell, D. P., Booth, B. B. B., Nicholson, S. E. & Good, P. Reconciling past and future  
300 rainfall trends over East Africa. *J. Clim.* **28**, 9768–9788 (2015).
- 301 29. Jones, B. & O’Neill, B. C. Spatially explicit global population scenarios consistent with  
302 the Shared Socioeconomic Pathways. *Environ. Res. Lett.* **11**, (2016).
- 303 30. Cai, W. *et al.* Increased frequency of extreme La Niña events under greenhouse warming.  
304 *Nat. Clim. Chang.* **5**, 132–137 (2015).
- 305 31. Cai, W. *et al.* Increasing frequency of extreme El Niño events due to greenhouse warming.  
306 *Nat. Clim. Chang.* **4**, 111–116 (2014).
- 307 32. Takahashi, H. G. *et al.* Response of the asian summer monsoon precipitation to global  
308 warming in a high-resolution global nonhydrostatic model. *J. Clim.* **33**, 8147–8164  
309 (2020).
- 310 33. FAOSTAT. Detailed Trade Matrix. Food and Agriculture Organization of the United  
311 Nations. Available online at: <http://www.fao.org/faostat/en/#data/TM> (accessed March 1,  
312 2021). (2020).
- 313 34. Dalin, C., Wada, Y., Kastner, T. & Puma, M. J. Groundwater depletion embedded in  
314 international food trade. *Nature* **543**, 700–704 (2017).
- 315 35. D’Odorico, P. *et al.* Global virtual water trade and the hydrological cycle: Patterns,  
316 drivers, and socio-environmental impacts. *Environ. Res. Lett.* **14**, (2019).
- 317 36. Graham, N. T. *et al.* Future changes in the trading of virtual water. *Nat. Commun.* **11**, 1–7  
318 (2020).
- 319 37. Barnston, A. G., Tippett, M. K., L’Heureux, M. L., Li, S. & Dewitt, D. G. Skill of real-  
320 time seasonal ENSO model predictions during 2002-11: Is our capability increasing? *Bull.*  
321 *Am. Meteorol. Soc.* **93**, 631–651 (2012).

322

## 323 **Methods**

324 **Datasets.** We use the 40-member Community Earth System Model Version-1 (CESM1) Large  
325 Ensemble Simulations (LENS) to examine the drivers of historical (1971-2000) compounding  
326 droughts and their projected changes (2071-2100) under the RCP8.5 scenario<sup>38</sup>. Each ensemble  
327 member of the CESM-LENS differs only in its initial atmospheric conditions and has identical  
328 external forcing, thereby providing an opportunity to investigate the influence of internal  
329 variability under different climate conditions. CESM demonstrates high skill in reproducing the  
330 observed global precipitation patterns, ENSO characteristics (e.g., intensity, frequency and  
331 related global teleconnections)<sup>30,31,39</sup>..

332 We use observed monthly precipitation data for 1981–2019 from the Climate Hazards Group  
333 Infrared Precipitation with Stations (CHIRPS) version 2<sup>40</sup> to estimate the Shannon Entropy  
334 index<sup>41</sup>, which is used to identify the regions of high variability in the summer precipitation.  
335 CHIRPS combines satellite-based precipitation estimates with in-situ observations and models of  
336 terrain-based precipitation to provide spatially fine and continuous data<sup>40</sup>. For the calculation of  
337 changes in population and agricultural land exposures, historical (for the year 2000) and  
338 projected future population (for the year 2100) at 1-km spatial resolution<sup>42</sup> <  
339 [https://sedac.ciesin.columbia.edu/data/set/popdynamics-1-km-downscaled-pop-base-year-](https://sedac.ciesin.columbia.edu/data/set/popdynamics-1-km-downscaled-pop-base-year-projection-ssp-2000-2100-rev01)  
340 [projection-ssp-2000-2100-rev01](https://sedac.ciesin.columbia.edu/data/set/popdynamics-1-km-downscaled-pop-base-year-projection-ssp-2000-2100-rev01)>, and crop and pastureland fraction (based on the year 2000)  
341 <<https://sedac.ciesin.columbia.edu/data/set/aglands-pastures-2000>> at 10-km spatial resolution<sup>43</sup>  
342 are obtained from the NASA Socioeconomic Data and Applications Center. We consider the  
343 population projections from all five Shared Socioeconomic Pathways (SSPs) to quantify the  
344 uncertainty in population exposure to compounding droughts under projected future warming.

345

346 **Selection of Regions.** We quantify compound droughts across 10 SREX regions: Amazon  
347 (AMZ), Central America (CAM), Central North America (CNA), East Africa (EAF), East Asia  
348 (EAS), East North America (ENA), South Asia (SAS), Southeast Asia (SEA), Tibetan Plateau  
349 (TIB), and West Africa (WAF). We consider these regions for the following reasons: (1) many  
350 of these regions are connected by the global summer monsoon systems and influenced by similar  
351 large-scale modes of variability<sup>27</sup>, (2) these receive the largest fraction of annual precipitation  
352 during the summer season (June – September; JJAS)<sup>22,27</sup> and exhibit strong variability in summer  
353 precipitation, and (3) these include several major breadbaskets and populations vulnerable to  
354 climate variability and change<sup>23</sup>.

355 To identify the sub-regions that exhibit high variability in summer precipitation, we estimate the  
356 observed Shannon Entropy Index<sup>41</sup> using monthly summer precipitation from the CHIRPS  
357 dataset. We only consider those regions that show high variability (entropy >4.86; median  
358 entropy values across the areas studied) in the monthly summer precipitation over at least 30% of  
359 their total area (Figure 1a). The Shannon Entropy  $H$  is estimated using the following equation<sup>44</sup>,

360

$$361 \quad H = -\sum p_i \log_2 p_i \quad (1)$$

362

363 where,  $p$  is the probability of each  $i^{\text{th}}$  value of the time series. The areas within each region that  
364 satisfy the Shannon entropy criterion compare well between observations (CHIRPS) and  
365 simulations (CESM) (Figures 1a, S6). The only exception is over AMZ where the extent of  
366 simulated area with high variability is relatively smaller than observed (Figure S6). Furthermore,  
367 CESM exhibits skills in simulating the compound droughts characteristics across these regions  
368 that have been described in Singh *et al*<sup>20</sup>.

369

370 **Drought Characteristics.** We use Standardized Precipitation Evapotranspiration Index (SPEI)  
371 to define drought<sup>45,46</sup>. SPEI is estimated using a simple climatic water balance, i.e., the difference  
372 between the accumulated summer season precipitation and evapotranspiration (ET)<sup>45</sup>. We  
373 compute ET as the sum of ground and canopy evaporation and transpiration for the present and  
374 future climates from CESM-LENS following the approach provided by Mankin *et al*<sup>47</sup>. To

375 construct SPEI, we follow a procedure similar to the Standardized Precipitation Index  
 376 calculations proposed by McKee *et al*<sup>48</sup>. We use a log-Logistic distribution to estimate the  
 377 probability distribution of P-ET instead of the Gamma distribution<sup>45</sup> that is used for SPI<sup>49</sup>. The  
 378 gamma distribution requires a variable with non-negative values, which makes it inappropriate  
 379 for SPEI estimation because the P-ET may yield negative values. Hence, we estimate the  
 380 probability of P-ET based on the widely used two-parameter Log-logistic distribution and then  
 381 transform it to a standard normal distribution to make it comparable across space and time<sup>45,46</sup>.  
 382 Future (2071–2100) SPEI calculations use historical (1971–2000) climate characteristics to  
 383 characterize changes in compound droughts relative to the historical climate.

384 We use the threshold of  $-1\sigma$  of the historical SPEI to classify a grid cell experiencing drought ( $<-$   
 385  $1\sigma$ ) in the historical and future climates. We define an individual drought over a region if the  
 386 fractional area experiencing drought conditions ( $\text{SPEI} < -1\sigma$ ) exceeds the 80<sup>th</sup> percentile of the  
 387 historical long-term average drought area. A compound droughts event is identified if at least  
 388 three of the ten SREX regions concurrently experience drought. Compound drought area is  
 389 defined as the fraction of the total area across the regions involved in compound droughts events.  
 390 Similarly, the compound droughts intensity is computed as average SPEI over drought-affected  
 391 areas across those regions. A compound drought event is classified as widespread when the  
 392 drought-affected area exceeds the 90<sup>th</sup> percentile of the historical long-term average area affected  
 393 by compound droughts (i.e.  $\sim 41\%$ ). Furthermore, these events are classified as severe (moderate)  
 394 when average SPEI across all drought-affected areas is below (above) the 10th percentile ( $\sim$   
 395  $-1.65$ ) of the historical long-term average SPEI over drought-affected areas during compound  
 396 droughts.

397

398 **Crop, pasture lands and population exposure.** There is a mismatch between the horizontal  
 399 grid spacing of climate data and cropland, pastureland and population datasets. Moreover, the  
 400 rate of population growth varies across space and depends on several local and global spatial  
 401 interactions<sup>29</sup>. Therefore, it is not appropriate to use interpolation methods to upscale the  
 402 population data to match  $\sim 1^\circ$  CESM grid cells. Therefore, instead of remapping, we aggregate  
 403 the population across the grid cells (at 1 km spatial resolution) that fall inside the  $\sim 1^\circ$  CESM grid  
 404 cells to calculate population exposure. We follow same procedure for crop and pasture lands.  
 405 Given the importance of cropland for food cultivation and pastureland for animals grazing, we  
 406 quantify the exposure of these land types to compound droughts. Cropland, pastureland and  
 407 population exposures are calculated as follows:

$$408 \quad \text{Cropland and pastureland exposure: } \frac{1}{N} \sum_{i=1}^n a_i \quad (1)$$

409

410 where,  $N$  is number of years,  $i$  indicates years with compound droughts events,  $a$  indicates the  
 411 total drought affected cropland or pastureland across the regions involved in the compound  
 412 droughts. Cropland and pastureland is based on the year 2000 and is fixed for both present and  
 413 future climates.

414

$$415 \quad \text{Population exposure: } \frac{1}{N} \sum_{i=1}^n p_i \quad (2)$$

416

417 Where,  $N$  is number of years,  $i$  indicates years with compound drought,  $p$  indicates the number of  
418 people experiencing drought across the regions involved in the compound droughts. We consider  
419 historical population based on year 2000 and projected future population based on year 2100  
420 under all five SSPs.

421  
422 **Large-scale Modes of Variability.** We define the ENSO index using the average summer (June  
423 to September; JJAS) sea surface temperatures anomalies (SSTA) over the Niño3.4 region (5S-  
424 5N, 170W-120W)<sup>50</sup>. We remove the forced climate change component from each member of the  
425 large ensemble by subtracting the time-varying mean of all ensemble members, as follows:

$$426 \quad SSTA_{i,j} = SST_{i,j} - \left(\frac{1}{40} \sum_{j=1}^{j=40} SST_j\right)_i \quad (3)$$

427  
428 where  $i$  represents the year and  $j$  represents the ensemble member. El Niño and La Niña are  
429 defined as exceedances of  $\pm 0.5\sigma$ , where the standard deviation ( $\sigma$ ) is estimated using the  
430 historical ENSO index values (1971–2000)<sup>20</sup>.

431 **Statistical Significance of the changes in compound droughts.** We employ the non-parametric  
432 permutation test to assess the statistical significance of the differences in mean compound  
433 droughts characteristics in the historical and future climates<sup>51</sup>. We first quantify the test statistic  
434 (i.e. difference in the means of the distributions of compound droughts characteristics) from the  
435 two original historical and future distributions and then estimate an empirical distribution of the  
436 test statistic by randomly permuting the samples from the two distributions and re-estimating the  
437 test statistic from the resampled distributions, 10,000 times. If the original test statistic is higher  
438 (lower) than the 95<sup>th</sup> (5<sup>th</sup>) percentile of the empirical distribution, we consider the mean of  
439 compound droughts characteristics between historical and future climates to be significantly  
440 different at the 5 percent significance level.

#### 441 **Data availability**

442 All datasets used in the manuscript are publicly available and their sources are provided in the  
443 “Methods” section.

#### 444 **Code availability**

445 The scripts developed to analyze these datasets can be made available on request from the  
446 corresponding author.

#### 447 **References**

- 448  
449 38. Kay, J. E. *et al.* The community earth system model (CESM) large ensemble project : A  
450 community resource for studying climate change in the presence of internal climate  
451 variability. *Bull. Am. Meteorol. Soc.* **96**, 1333–1349 (2015).  
452 39. Fasullo, J. T., Otto-Bliesner, B. L. & Stevenson, S. ENSO’s Changing Influence on  
453 Temperature, Precipitation, and Wildfire in a Warming Climate. *Geophys. Res. Lett.* **45**,

- 454 9216–9225 (2018).
- 455 40. Funk, C. *et al.* The climate hazards infrared precipitation with stations - A new  
456 environmental record for monitoring extremes. *Sci. Data* **2**, 1–21 (2015).
- 457 41. Shannon, C. . A mathematical theory of communication. *Bell. Syst. Tech. J.* **27**, 623–656  
458 (1948).
- 459 42. Gao, J. Global 1-km Downscaled Population Base Year and Projection Grids Based on the  
460 Shared Socioeconomic Pathways, Revision 01. *Palisades, NY NASA Socioecon. Data*  
461 *Appl. Cent.* (2020).
- 462 43. Ramankutty, N., Evan, A. T., Monfreda, C. & Foley, J. A. Global Agricultural Lands:  
463 Croplands, 2000. *Palisades, NY NASA Socioecon. Data Appl. Cent.* (2010).
- 464 44. Mishra, A. K., Özger, M. & Singh, V. P. An entropy-based investigation into the  
465 variability of precipitation. *J. Hydrol.* **370**, 139–154 (2009).
- 466 45. Vicente-Serrano, S. M., Beguería, S. & López-Moreno, J. I. A multiscalar drought index  
467 sensitive to global warming: The standardized precipitation evapotranspiration index. *J.*  
468 *Clim.* **23**, 1696–1718 (2010).
- 469 46. Beguería, S., Vicente-Serrano, S. M., Reig, F. & Latorre, B. Standardized precipitation  
470 evapotranspiration index (SPEI) revisited: Parameter fitting, evapotranspiration models,  
471 tools, datasets and drought monitoring. *Int. J. Climatol.* **34**, 3001–3023 (2014).
- 472 47. Mankin, J. S. *et al.* Influence of internal variability on population exposure to  
473 hydroclimatic changes. *Environ. Res. Lett.* **12**, (2017).
- 474 48. McKee, B. T., Nolan, D. J. & John, K. THE RELATIONSHIP OF DROUGHT  
475 FREQUENCY AND DURATION TO TIME SCALES. *Eighth Conf. Appl. Climatol.*  
476 179–184 (1993) doi:10.1002/jso.23002.
- 477 49. Mishra, A. K. & Singh, V. P. A review of drought concepts. *J. Hydrol.* **391**, 202–216  
478 (2010).
- 479 50. Rayner, N. A. *et al.* Global analyses of sea surface temperature, sea ice, and night marine  
480 air temperature since the late nineteenth century. *J. Geophys. Res. D Atmos.* **108**, (2003).
- 481 51. Good, P. I. *Permutation tests: A practical guide to resampling methods for testing*  
482 *hypotheses.* (Springer-Verlag, 1994).

## 483 **Acknowledgements**

484 We would like to thank the National Center for Atmospheric Research (NCAR) and Climate  
485 Hazards Center UC Santa Barbara for archiving and enabling public access to their data. We  
486 thank Washington State University for the startup funding that has supported J.S. and D.S.  
487 W.B.A. acknowledges funding from Earth Institute Postdoctoral Fellowship. M.A. was  
488 supported by the National Climate-Computing Research Center, which is located within the  
489 National Center for Computational Sciences at the ORNL and supported under a Strategic  
490 Partnership Project, 2316-T849-08, between DOE and NOAA. This manuscript has been co-  
491 authored by employees of Oak Ridge National Laboratory, managed by UT Battelle, LLC, under  
492 contract DE-AC05-00OR22725 with the U.S. Department of Energy (DOE). The publisher, by  
493 accepting the article for publication, acknowledges that the United States Government retains a  
494 non-exclusive, paid-up, irrevocable, world-wide license to publish or reproduce the published

495 form of this manuscript, or allow others to do so, for United States Government purposes. The  
496 Department of Energy will provide public access to these results of federally sponsored research  
497 in accordance with the DOE Public Access Plan ([http://energy.gov/downloads/doe-public-  
498 access-plan](http://energy.gov/downloads/doe-public-access-plan)).  
499

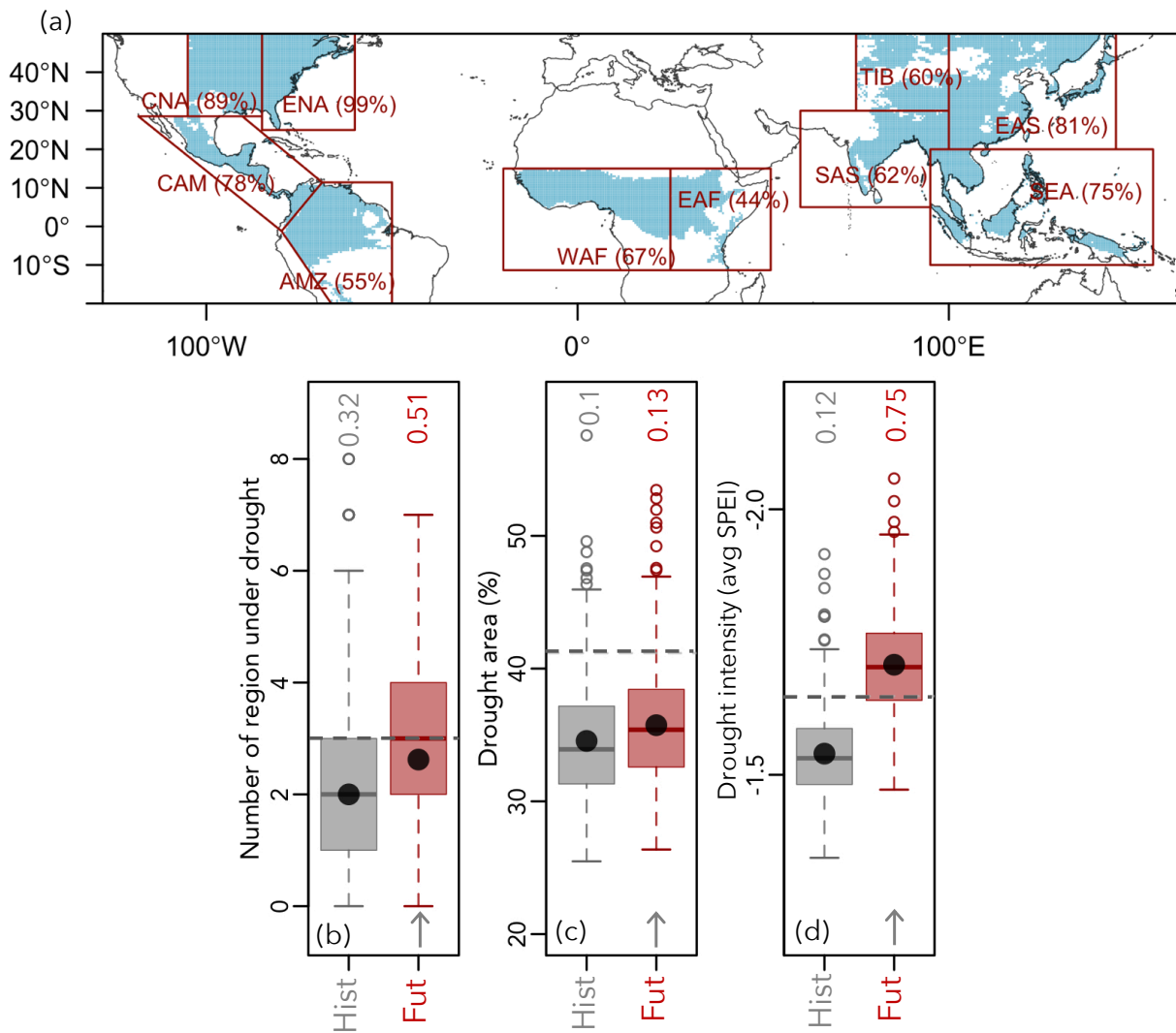
500

501 **Author Contributions**

502 All authors contributed to the design of the study. J.S. collected the data and performed the  
503 analyses. All authors were involved in discussions of the results. J.S. and D.S. wrote the  
504 manuscript with feedback from all authors.  
505

506 **Competing Interests**

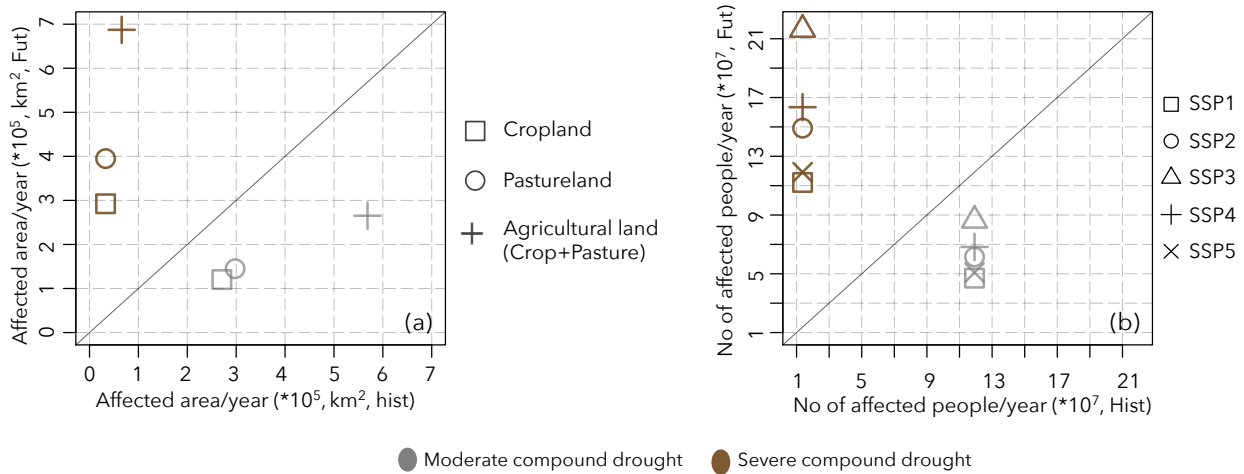
507 The authors declare no competing interests.  
508  
509  
510  
511  
512  
513  
514  
515  
516  
517  
518  
519  
520  
521  
522  
523  
524  
525  
526  
527  
528  
529  
530  
531  
532  
533  
534  
535  
536  
537  
538  
539  
540



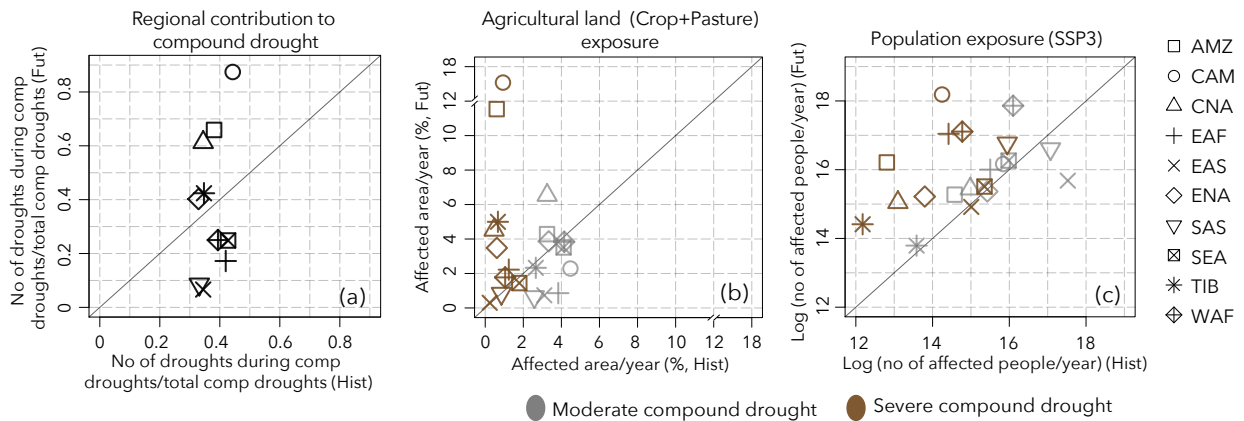
543

544 **Figure 1. Historical and future characteristics of compound droughts.** (a) Map showing the  
545 10 SREX regions (red line) considered in this study. Red text indicates the fraction of each  
546 SREX region with high entropy values [entropy > 4.86, which is the median entropy value across  
547 10 SREX regions] (teal color) estimated from observed CHIRPS precipitation data (1981-2018)  
548 at 0.25° resolution. (b) The distribution of the number of regions under drought in historical  
549 (grey box) and future (red box) climate. Figures (c) and (d) show the distribution of drought area  
550 and intensity associated with compound droughts. Horizontal grey dashed lines indicate the  
551 thresholds used to define (b) compound (i.e.,  $\geq 3$  regions under drought, gray line) drought, (c)  
552 widespread (i.e., events with >90th percentile of total area ( $\sim 41\%$ ) across all 10 regions  
553 concurrently affected by drought), and (d) severe (i.e., average SPI across all drought affected  
554 areas < 10th percentile ( $\sim -1.65$ ), gray line) compound drought. Text above the boxplots in panel  
555 (b) indicates the probability of compound droughts, (c) indicates the probability of experiencing  
556 widespread compound droughts and (d) indicates the probability of experiencing severe

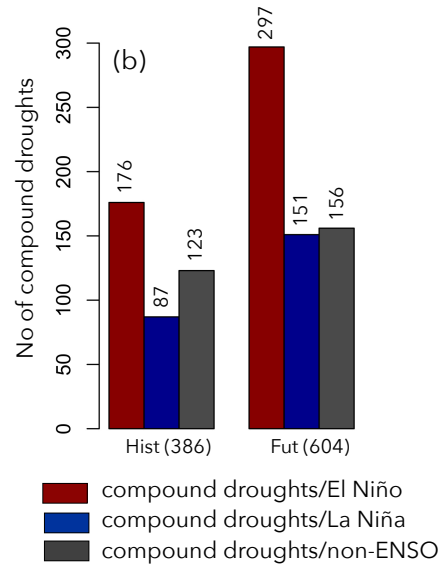
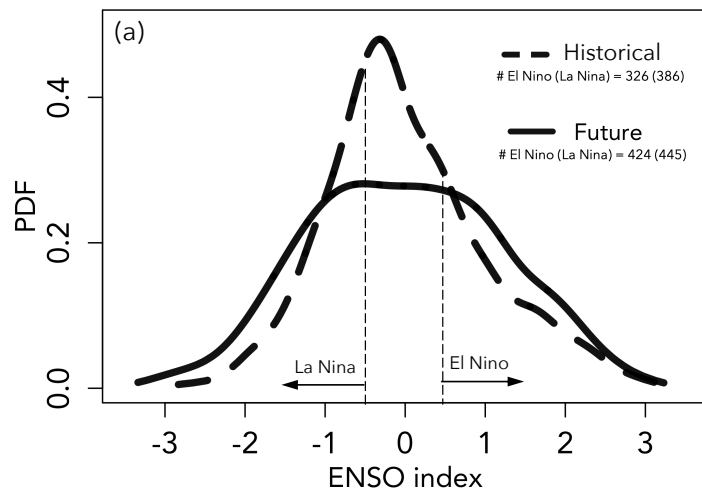
557 compound droughts. Gray arrows at the bottom of the panels indicate significant differences (at  
 558 5% significance level) in the future distribution of drought regions, drought area and intensity  
 559 relative to the historical climate. Black dots show the mean of the distribution in each boxplot.  
 560



561  
 562 **Figure 2. Crop, pasture lands, and population exposure to compound droughts.** (a)  
 563 Agricultural area and (b) population exposure across the regions under compound droughts. X-  
 564 and Y- axes indicate the average cropland/pastureland/agricultural land (combined cropland and  
 565 pastureland) area and population per year exposed to compound droughts in the historical and  
 566 future climate, respectively. A 45-degree solid line is used to compare exposure between  
 567 historical and future climates at 1:1 in each panel.  
 568  
 569

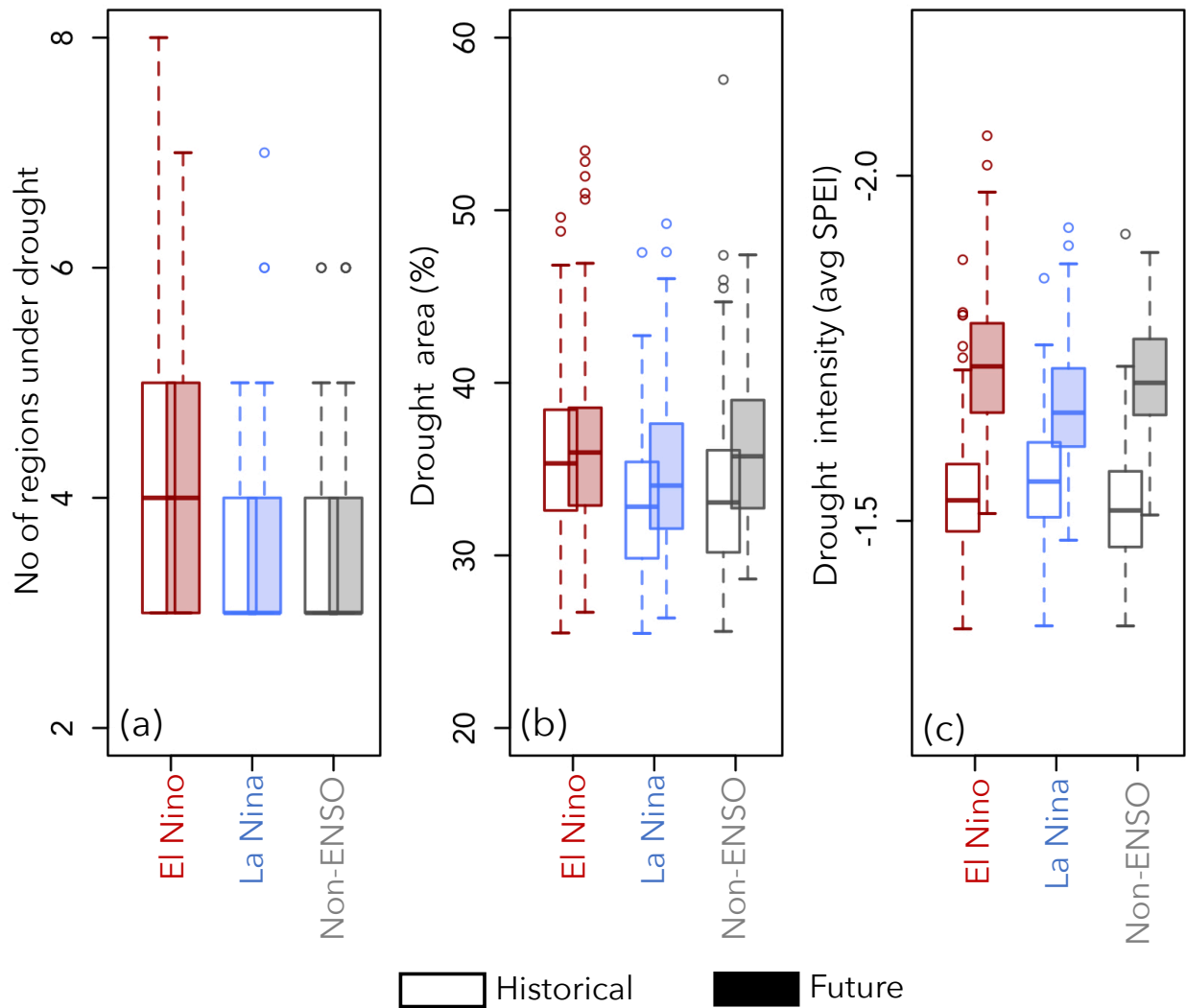


570  
 571 **Figure 3. Contribution of regions to compound droughts and to agricultural area and**  
 572 **population exposure to compound drought.** (a) X- and Y- axes indicate the fraction of  
 573 instances in which a particular region experiences drought during compound droughts in the  
 574 historical and future climates, respectively. (b) Average agricultural land (total cropland and  
 575 pastureland) (in %) exposure to compound droughts in historical and future climates. (c) Average  
 576 number of people exposed to compound droughts in historical and future climates under SSP3.  
 577  
 578



579

580 **Figure 4. Changes in the frequency of ENSO events and compound droughts in future**  
 581 **climate.** (a) The probability distribution function (PDF) of the ENSO index. The text in the inset  
 582 indicates the number of El Niño (ENSO > 0.5SD) and La Niña (ENSO < -0.5SD) events in the  
 583 historical and future climate. (b) The count of compound droughts associated with El Niño  
 584 events, La Niña events and non-ENSO drivers. The text on the x-axis indicates the total number  
 585 of compound droughts in the historical and future climates. The text on top of each bar indicates  
 586 the number of compound droughts that occur with the various physical drivers.



587

588 **Figure 5. Influence of ENSO and non-ENSO drivers on compound drought characteristics.**

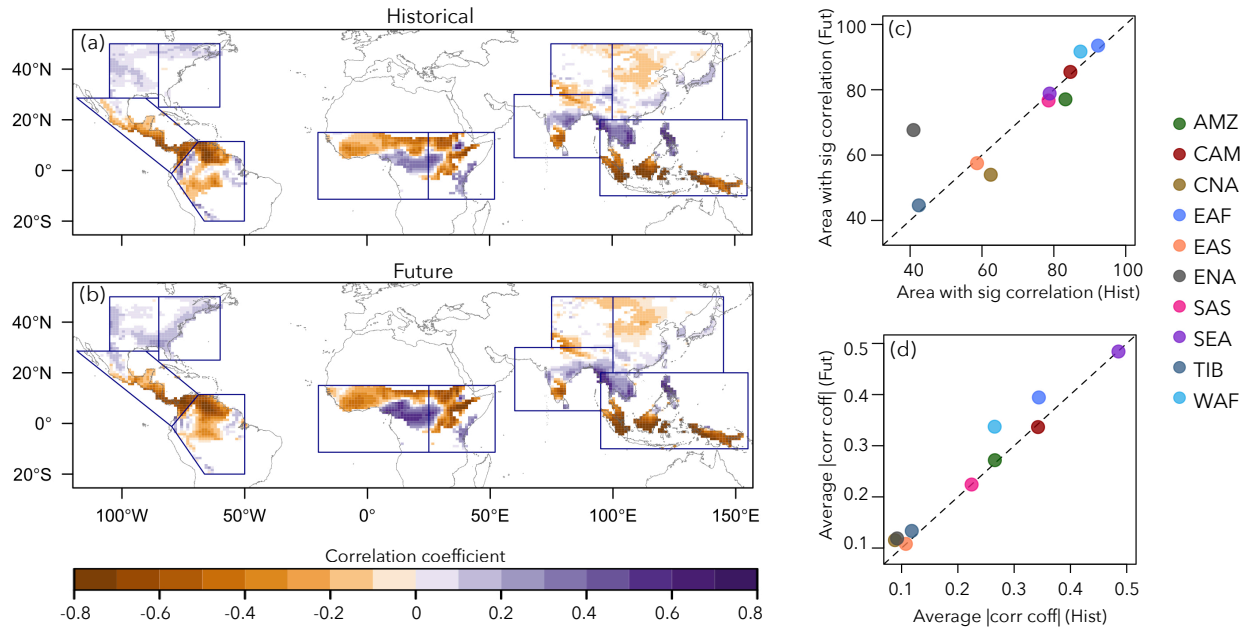
589 The distribution of (a) number of regions under drought, (b) drought area, and (c) drought

590 intensity associated with compound droughts related to various physical drivers noted below

591 each boxplot.

592

593



594

595 **Figure 6. Changes in the ENSO teleconnections with SPEI over land in future climate.**

596 Correlation between ENSO and SPEI in the (a) historical and (b) future climate. (c) Changes in  
 597 the area with significant (at 5% significance level) correlation between ENSO and SPEI across  
 598 all regions in the future relative to the historical climate. (d) the changes in the strength of  
 599 correlation (average absolute correlation coefficient) between ENSO and SPEI across all regions  
 600 in the future relative to historical climate.

601